Electrosprayed mesoporous particles for improved aqueous solubility of a poorly water soluble anticancer agent: *in vitro* and *ex vivo* evaluation

Elshaimaa Sayed[1,2], Christina Karavasili[3], Ketan Ruparelia[1], Rita Haj-Ahmad[1], Georgia Charalambopoulou[4], Theodore Steriotis[4], Dimitra Giasafaki[4], Paul Cox[5], Neenu Singh[6], Lefki-Pavlina N. Giassafaki[3], Aggeliki Mpenekou[3], Catherine, K. Markopoulou[3], Ioannis S. Vizirianakis[3], Ming-Wei Chang[7,8], Dimitrios G. Fatouros[3,*], Zeeshan Ahmad[1,*]

[1]Leicester School of Pharmacy, De Montfort University, Leicester, LE1 9BH, UK,

[2]Department of Pharmaceutics, Faculty of Pharmacy, Minia University, Minia, Egypt.

[3]Department of Pharmacy, Aristotle University of Thessaloniki. GR-54124 Thessaloniki, Greece

[4]National Center for Scientific Research "Demokritos", 15341 Agia Paraskevi Attikis, Greece

[5]School of Pharmacy and Biomedical Sciences and Institute of Biomedical and Biomolecular Sciences, University of Portsmouth, Portsmouth, PO1 2DT, UK

[6]Faculty of Health and Life Sciences, School of Allied Health Sciences, De Montfort University, The Gateway, Leicester LE1 9BH, UK

[7]College of Biomedical Engineering and Instrument Science, Zhejiang University, Hangzhou 310027, China

[8]Zhejiang Provincial Key Laboratory of Cardio-Cerebral Vascular Detection Technology and Medicinal Effectiveness Appraisal, Zhejiang University, Hangzhou 310027, China

Corresponding authors: Dimitrios G.Fatouros e-mail: dfatouro@pharm.auth.gr, Zeeshan Ahmad e-mail: zahmad@dmu.ac.uk

1.1. Methods

1.2. Chalcone Synthesis reaction

The Claisen-Schmidt condensation typically involves equimolar quantities of the benzaldehyde and an acetophenone in the presence of alcoholic alkali (Scheme 1):

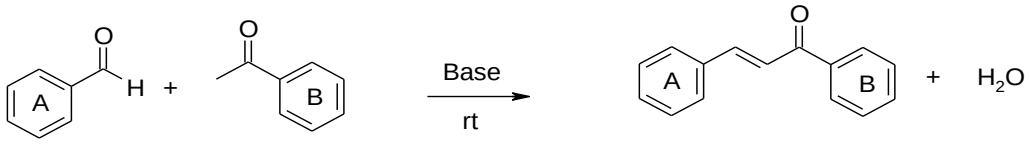

Scheme S1. Chalcone synthesis by classic base-catalysed reaction (Claisen-Schmidt).

1.3. KAZ3 structure characterization

The structure of the formed chalcone was confirmed using an array of different analytical methods including nuclear magnetic resonance (NMR), mass spectroscopy (MS), Fourier transform infrared spectroscopy (FTIR) and thin layer chromatography (TLC). The ^{1}H-NMR and ^{13}C-NMR spectra were recorded on a 400 MHz super-conducting Bruker Spectrometer at 30 °C. Tetramethylsilane (TMS) was used as an internal standard. Chemical shifts are reported in δ units relative to the TMS signal and coupling constants (*J*) expressed in Hertz (Hz).^{1}H-NMR information is provided in the following format: number of protons, multiplicity, coupling constant (where necessary) and assignment. Multiplicities are reported as follow; s=singlet, d=doublet, t=triplet, q=quartet, dd=doublets of doublet, m=multiplet. Infrared spectra (IR) were recorded using potassium bromide disks on a Perkin-Elmer 298 Spectrophotometer. Mass spectra and Accurate mass were recorded on a Micromass Quattro II Low Resolution Triple Quadruple Mass Spectrometer (EPSRC National Mass Spectrometry Service Centre, Swansea UK). Melting points (uncorrected) were determined on a Gallenkamp melting point apparatus in open glass capillary tubes. Thin layer chromatography (TLC) was performed on Merck Aluminium Sheet Silica Gel $60f_{254}$ coated plates. The TLC

plates visualised under Multiband UVGL-58 UV-254/366 nm UV light and stained with 2,4-dinitrophenylhydrazine (DNP to stain for the carbonyl group) or iodine absorbed on sand or phosphomolybdic acid (PMA). Silica gel (Fluka Silica 60; standard 30-45 μ fine grade 20-45 μ) was used for Flash Column Chromatography. Elemental analyses (CHN) were performed on a CE440 elemental analyser by Warwick Analytical Services and were within ± 0.4 % of the theoretical values, unless otherwise stated.

1.4. Structural characterization of silica hosts

The small angle X-ray scattering (SAXS) patterns of the mesoporous silica samples (MCM-41, SBA-15) were recorded on a Rigaku R-AXIS IV Imaging Plate Detector mounted on a Rigaku RU-H3R Rotating Copper Anode X-ray Generator (λ=1.54 Å). The pore structure of SBA-15 and MCM-41 silica samples was studied by means of N_2 adsorption-desorption isotherms at 77 K. The experiments were performed on an automated manometric instrument (Autosorb-1MP, Quantachrome Instruments) after outgassing the samples (~30 mg) at 250 ^{o}C overnight under high vacuum. BET areas were calculated by the pertinent approximation and consistency criteria [42], while the pore volumes of MCM-41 and SBA-15 samples were determined from the N_2 uptake plateau value at high relative pressures (p/p0~0.96) by assuming that the adsorbed fluid has liquid N_2 density. Pore size distributions were deduced by using the N2-silica QSDFT (Quenched Solid Density Functional Theory) kernels.

1.5. Preliminary drug concentration determination

A preliminary study was conducted to investigate the suitable drug concentration in the initial suspensions of mesoporous silica before conducting electrospraying or solvent impregnation as loading methods. SBA-15 (6 mg/mL) was suspended in different drug

solutions with three different drug concentrations (2 mg/mL, 6 mg/mL, 12 mg/mL). Both loading methods were applied on the prepared suspensions. The produced loaded formulations were analyzed for their drug content using UV spectrophotometry and drug crystallinity using XRD.

1.6. Particle size distribution

The particle size distributions of SBA-15, MCM-41, FS and the drug loaded formulations were analysed using laser diffraction size analysis (NanoBrook Omni Particle Sizer and Zeta Potential Analyzer, Brookhaven Instruments, UK). Two mg of each sample were suspended in 2 mL distilled water and were sonicated for 5 minutes. The particle size distribution was an average of five repetitions. The average values of D10, D50 and D90 were taken as the mean diameter. The lognormal size distribution was used to determine the size uniformity by calculating the span value. The span value is a parameter that is used to assess the width of particle size distribution and was calculated using the following equation

$$Span = \frac{D90 - D10}{D50} \qquad [2]$$

Where D10, D50 and D90 are the sizes for which 10 %, 50 % and 90 % of the population (distribution) lies below, respectively. The higher the span value, the wider the particle size distribution.

1.7. ζ-potential studies

Zeta potential of the pristine and the drug loaded samples was measured in phosphate buffer saline (PBS) solution. The zeta potential values of the silica particles dispersions in acetone and ethanol were also measured. All experiments were performed using

NanoBrook Omni Particle Sizer and Zeta Potential Analyzer (Brookhaven Instruments, UK) and were repeated three times.

1.8. Fourier transform infrared spectroscopy (FTIR)

Chemical bonding and interactions of MCM-41, SBA-15, FS and the drug loaded formulations were investigated using Perkin Elmer FTIR (Perkin Elmer with the software Bruker Alpha Opus 27). The IR spectra were obtained using the ATR technique (attenuated total reflection) on diamond crystal over the range of 4000 - 400 cm^{-1} after 30 scans with a resolution of 4 cm^{-1}.

1.9. HPLC analysis

A Shimadzu HPLC system series LC-20A was used for drug quantification consisting of a LC-20AD module pump, a SIL-10ADVP auto sampler and a UV-Diode array detector adjusted at 346 nm. Elution was performed on a Discovery® HS C18 (15 cm x 4.6 mm, 5µm) column using acetonitrile: water (60:40 v/v) as the mobile phase with a flow rate of 1.0 mL/min and an injection volume of 90 µL at 346 nm. The calibration curve was linear (R^2 =0.998) in the concentration range evaluated (0.5 - 4 µg/mL).

2. Results

2.1. KAZ3 Structure characterization

The chemical structure of the drug is shown in figure S1. The purity of the product was determined by TLC and elemental analysis. The product was also characterized by proton & carbon-13 NMR, infrared spectroscopy and mass spectrometry. The trans geometry of the alkene double bond was confirmed using 1H NMR, where the alkene protons appeared as a characteristic set of two doublets between 6.0 - 8.0 ppm having

coupling constants between 15 and 20 Hz, typical of a trans isomer Figure S2A. Coupling constants for cis alkene protons are 5-12 Hz. Coupling constants indicate the interaction between nuclei transmitted through intervening electrons. Aromatic proton-proton spin coupling constants gave information of whether the coupling protons are in ortho (Jab 7-10 Hz), meta (Jab 2-3 Hz) or para position (Jab 0-1 Hz) to each other. The infrared spectrum of KAZ3 (Figure S2C) shows absorption bands at ~1650-1660 cm^{-1} related to the α, β-unsaturated carbonyl group (=C–C=O), which is characteristic of chalcones. The vibration of the unsaturated C=C bond (enone group) resulted in an absorption peak at 1590 cm^{-1}, while the absorption band of =C–H appeared at 3005 cm^{-1}. The variance in absorption of the carbonyl group of chalcones is due to the presence of the electron donating methoxy groups in the phenyl ring. The asymmetrical stretching of the C-O-C bond in the methyl ether groups appeared around 1260 cm^{-1} with a symmetrical stretching band around 1020 cm^{-1}. A distinct absorption at about 1600 cm^{-1} is likely due to the presence of the aromatic carbon ring. The peaks in the range of 2800 cm^{-1} to 3000 cm^{-1} correspond to benzene C–H stretching. Mass spectra in low ionisation mode (EI, MALDI or FAB) gave either M+ or (M+1)+ peaks of appropriate m/z values with (M-CH3)+ as the common fragment, whereas methoxy groups were also present. Accurate mass analysis confirmed the expected molecular formula.

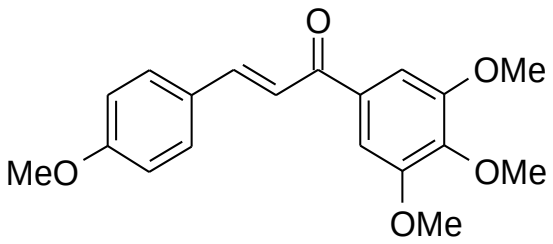

Figure S1. Chemical structure of (E)-3-(4-methoxyphenyl)-1-(3,4,5-rimethoxyphenyl)-prop-2-en-1-one (KAZ3).

Yellow crystals (1.96 g, 89%), TLC:Rf 0.54 (ethyl acetate/ petroleum ether 4:6), m/z [FAB+] (329 [M+H]+, 100%), □max (KBr) /cm-1 1653 (C=O), δH (CDCl3), 3.85 (3H, s, OMe), 3.95 (9H, s, 3xOMe), 6.95 (2H, d, ArH), 7.25 (2H, s, ArH), 7.37 (1H, d, CH=CH, J=17Hz), 7.61 (2H, d, ArH) 7.80 (1H, d, CH=CH, J=17Hz); □C (CDCl3), 55.4, 56.4, 61.0, 106.2, 114.5, 119.5, 127.7, 130.2, 133.9, 142.4, 144.6, 153.2, 157.5, 161.8, 189.3 (C=O); HRMS found [M+H]+ 329.1387, C18H17O5 requires [M+H]+ 329.1384; Anal. Calcd C19H20O5: C, 69.50; H, 6.14; Found C, 69.25; H, 6.24.

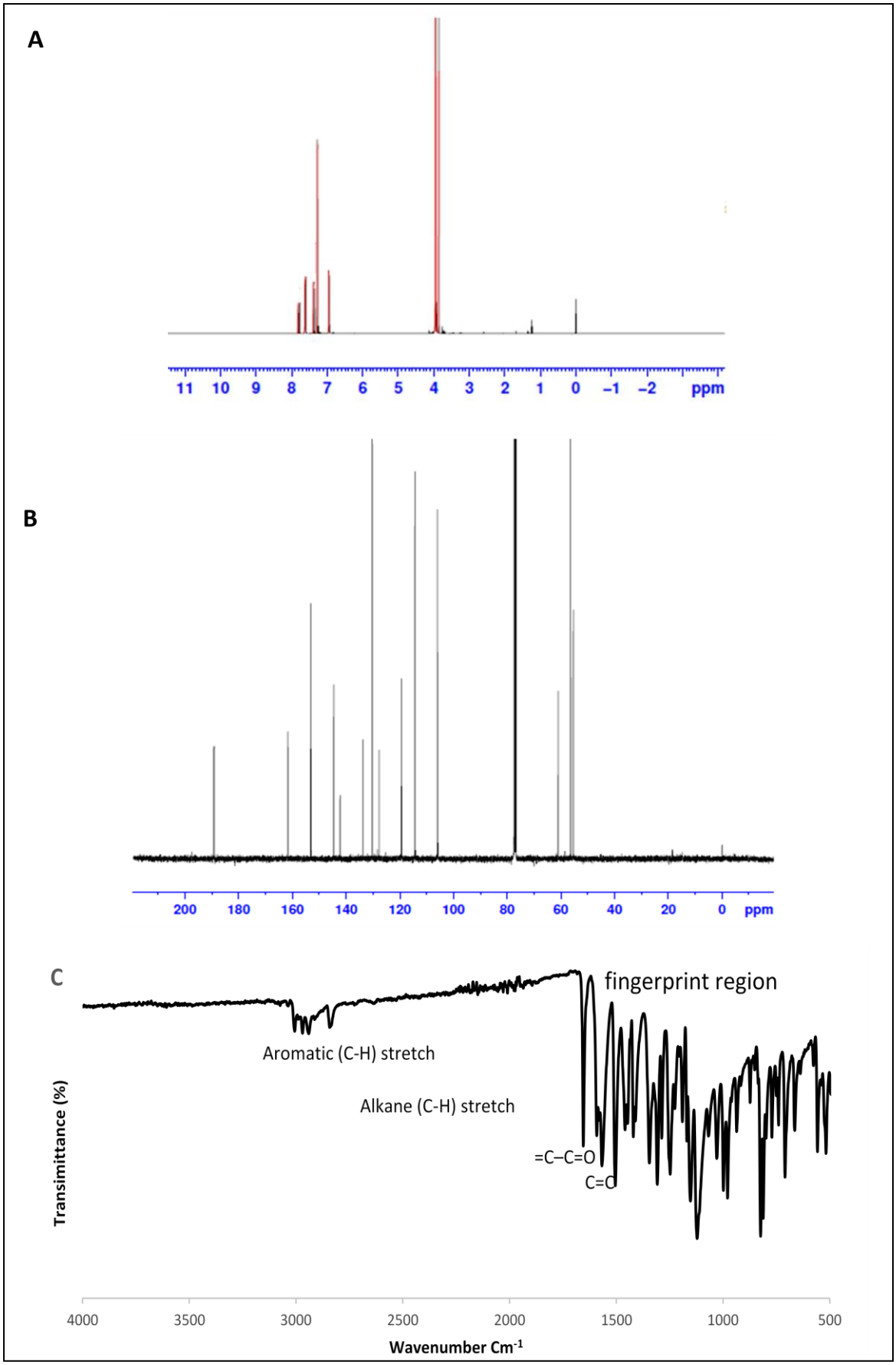

Figure S2. **A.** Proton NMR, **B.** Carbon NMR and **C.** Infrared spectra of KAZ3 chalcone.

2.2. Structural characterization of porous carriers

X-ray diffractograms (Figure S3) show that SBA-15 demonstrated three well resolved peaks, including an intense peak at 0.86° assigned to (10) diffraction, as well as two weaker peaks at 1.46° and 1.68° which are indexed to (11) and (20) diffractions, respectively, suggesting long-rage order. MCM-41 exhibited four distinct peaks; a strong peak at 2.18°, which corresponds to (10) diffraction and three weaker peaks at 3.72°, 4.28° and 5.72°, assigned to (11), (20) and (21) diffractions respectively, indicating a well-defined hexagonally ordered mesoporous structure. The structural parameters of the samples are summarized in Table S1. The nitrogen adsorption-desorption isotherms of both SBA-15 and MCM-41 samples Figure S3 were of type IV (based on IUPAC classification).

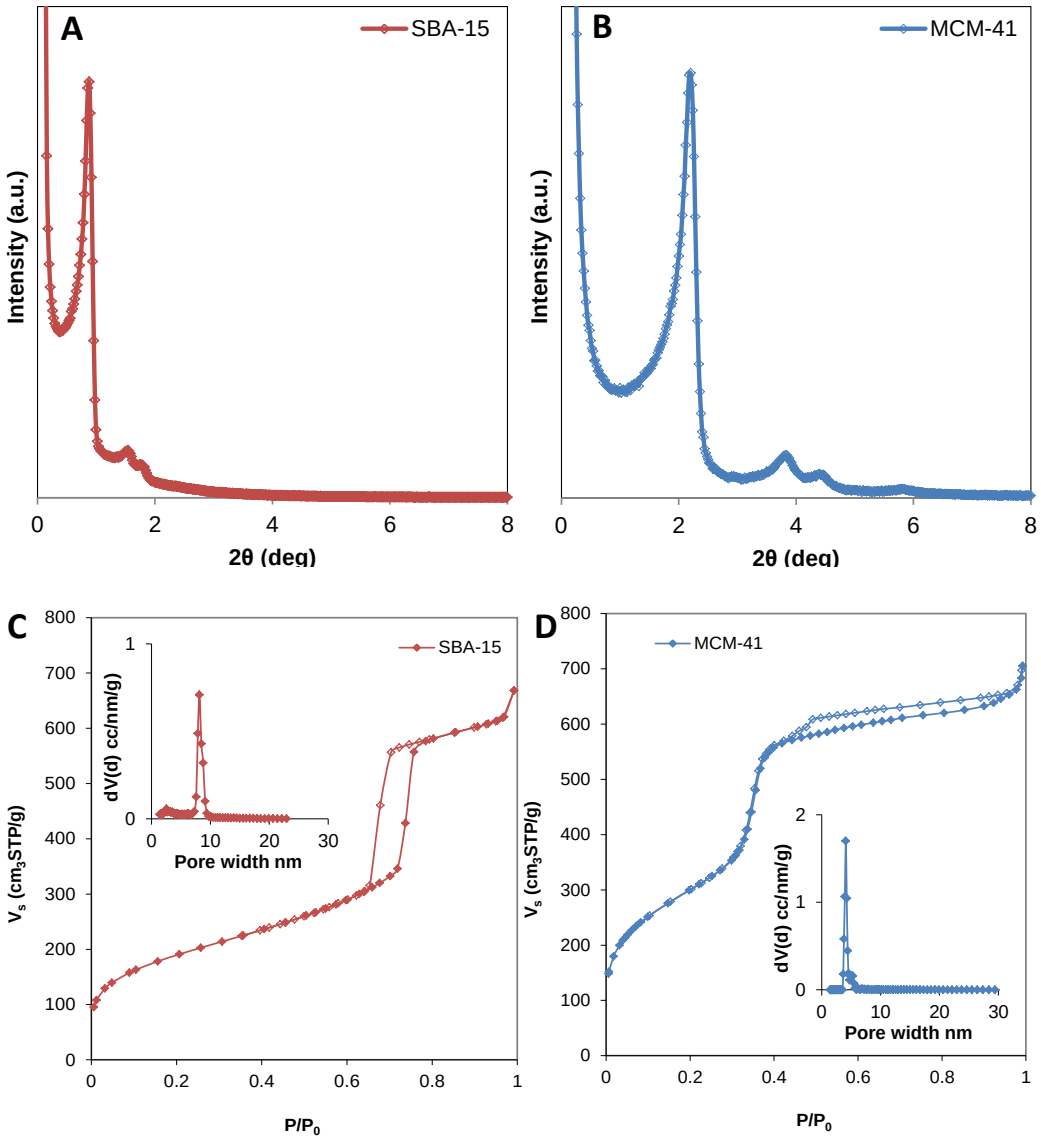

Figure S3. Small angle PXRD patterns of **A.** SBA-15 and **B.** MCM-41. N_2 adsorption (full symbols) – desorption (empty symbols) isotherms at 77 K of **C.** SBA-15 and **D.** MCM-41 and the respective pore size distributions (insets).

Table S1. Porous properties of the samples as determined from the N_2 adsorption / desorption isotherms and structural parameters estimated from PXRD measurements.

	S_{BET} (m^2/g)	TPV (cm^3/g)	D (nm)	d_{10} (nm)	a_0 (nm)	t_{wall} (nm)
SBA-15	680	1.0	8	10.3	11.8	3.7
MCM-41	1100	1.0	4	4.0	4.7	0.6

S_{BET}: BET area, TPV: total pore volume (at P/P_0=0.96), D: mean pore diameter (using QSDFT method on the adsorption branch), d_{10}: d spacing of the (10) reflections deduced from Bragg's equation, a_0: unit cell parameter for hexagonal symmetry according to the equation $a_0=2\cdot d_{10}/3^{1/2}$, t_{wall}: pore wall thickness obtained by subtracting pore size from the unit cell parameter ($t_{wall}=a_0-D$).

2.3 Preliminary drug concentration determination

A preliminary study was conducted to investigate the maximum drug content that can be loaded into mesoporous silica in the amorphous state using both loading methods (solvent impregnation and electrospraying). XRD was used to evaluate the crystallinity of the drug loaded in the different formulations. XRD pattern of KAZ3 was also obtained (Figure S4 A) confirming the drug's crystalline nature with four major diffraction peaks at 11.7 º, 17.3º, 21 º and 26.4 º.

A maximum loading efficiency (35.6 %) was achieved when using drug concentration of 2 mg/ml for samples prepared using the solvent impregnation method. However, further increasing the drug concentration decreased the encapsulation efficiency. EHDA method was able to achieve a high encapsulation efficiency at all tested drug concentrations. However, XRD analysis of electrosprayed formulations showed that the drug was entrapped in the amorphous form into the pores only when using drug concentrations of 2 mg/ml (Figure S4 B). A higher crystallinity in the produced formulations was observed by increasing the drug concentration to 6 mg/ml or 9 mg/ml. For the solvent impregnation method, increasing the drug concentration more than 2 mg/ml resulted in an increase in drug crystallinity in the resulting formulations (Figure S4 C). It can be concluded that a complete pore filling was achieved when suspending

mesoporous silica in drug solution of 2 mg/ml. As a result, 2 mg/ml was chosen as the initial drug concentration and 25 % w/w was set as a target loading for both loading methods.

Table S2. Encapsulation efficiency at different drug concentrations and drug to mesoporous silica ratios for both loading methods.

Loading Method	Drug concentration (mg/ml)	Drug: SBA-15 (Theoretical loading % w/w)	Encapsulation Efficiency (%)
Solvent impregnation	2	1:3 (25 %)	35.6 ± 3.2
Solvent impregnation	6	1:1 (50 %)	28.8 ± 0.14
Solvent impregnation	12	2:1 (66.6 %)	21.0 ± 1.2
Electrospraying	2	1:3 (25 %)	91.7 ± 0.4
Electrospraying	6	1:1 (50 %)	93.8 ± 16.6
Electrospraying	12	2:1 (66.6 %)	103.5 ± 6.1

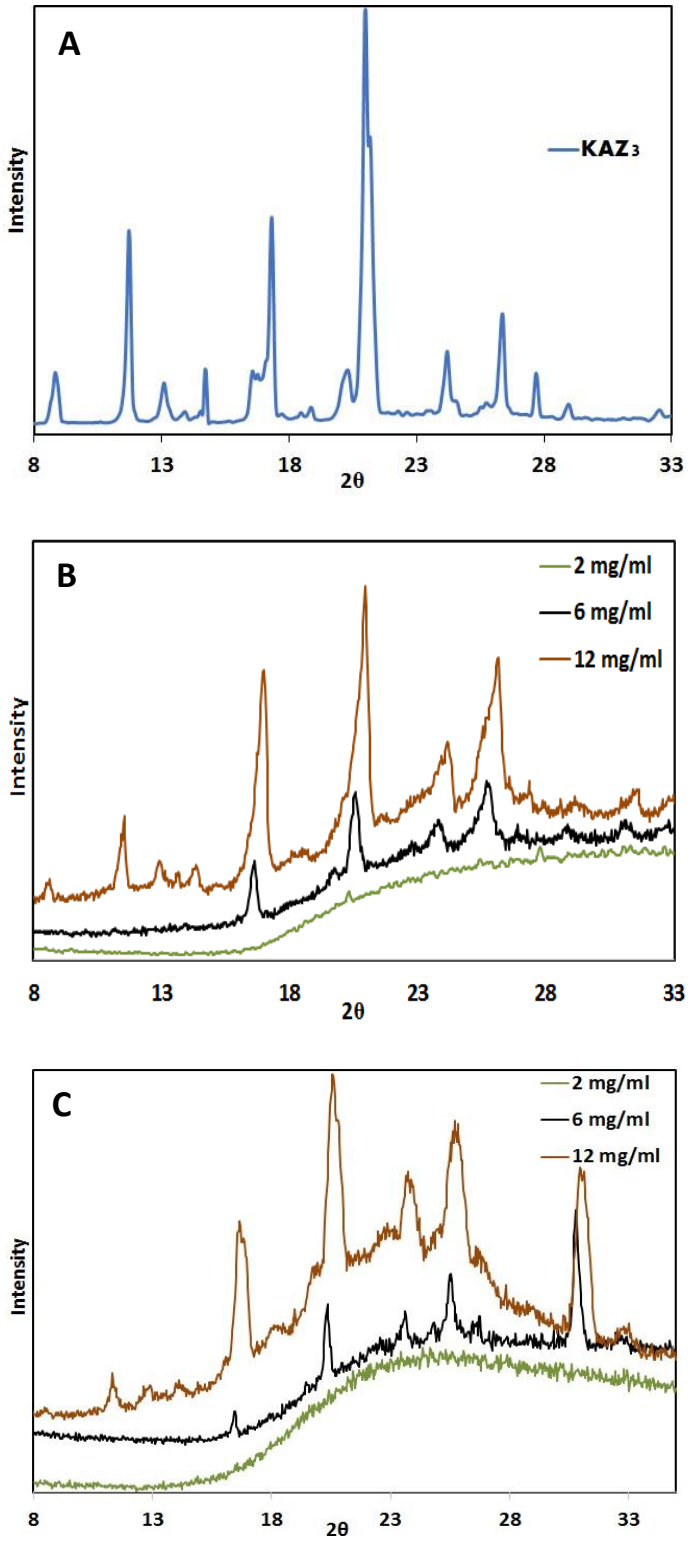

Figure S4. **A.** XRD pattern of pure KAZ3. Effect of initial drug concentration on the XRD patterns of KAZ3 loaded mesoporous silica using different drug loading methods **B.** electrospraying and **C.** solvent impregnation.

2.4 SEM

SEM images of the pristine silica particles and the prepared formulations are shown in Figure S5. SBA-15 (Figure S5 A) demonstrated rod-like particles with a diameter of approximately 0.45 μm and a length of ~1.1 μm. The resulting particulates showed an affinity to form longer fiber-like structures with lengths up to 10 - 22 μm. MCM-41 (Figure S5 F) exhibited compact, rough and irregular shaped particles (0.5-1 μm), as well as fiber-like structures, as in the case of pristine SBA-15. Non-porous FS (Figure S5 K) consisted of small irregular shaped particles (0.1 - 0.5 μm) that tend to agglomerate into coarse spherical clumps.

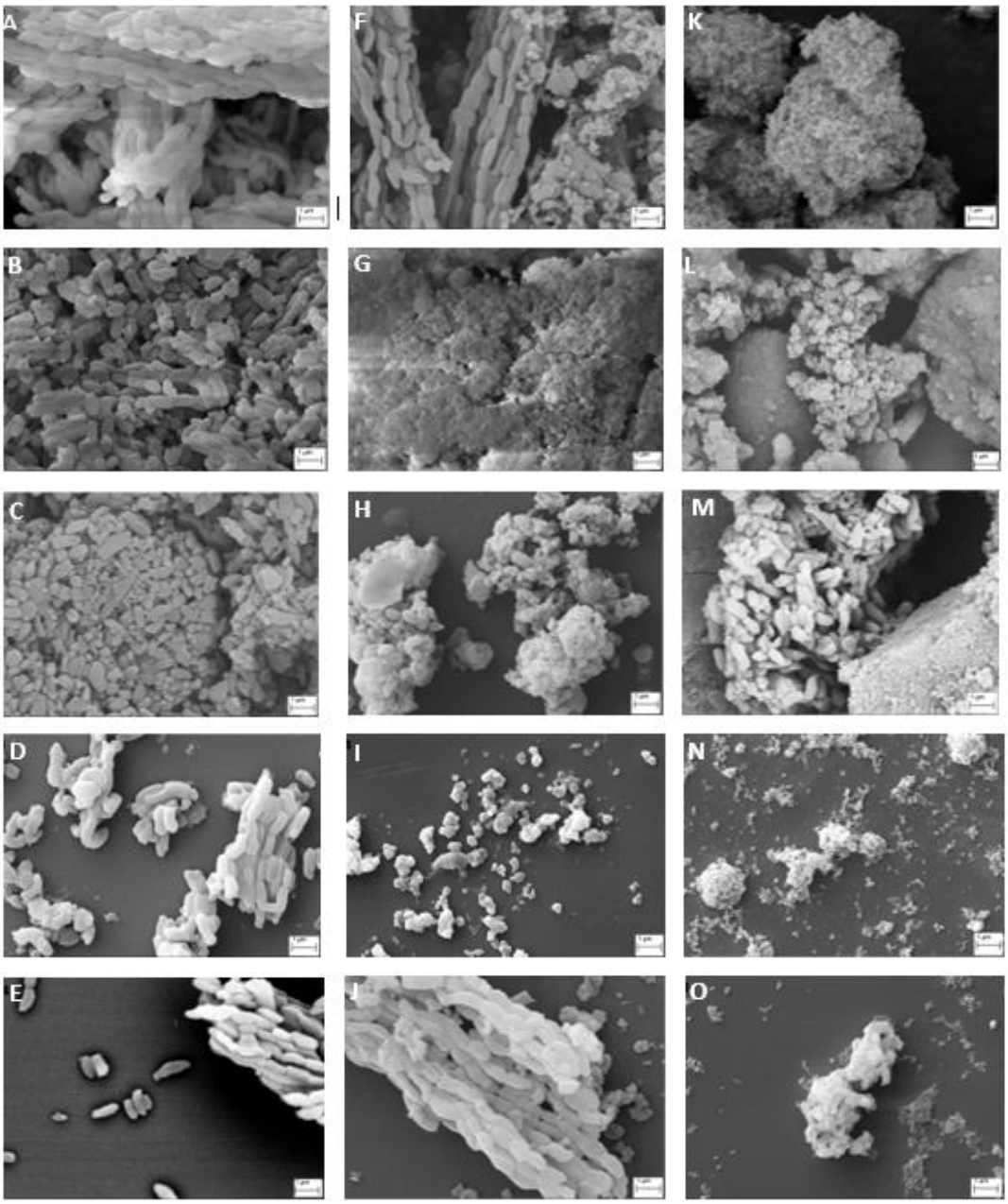

Figure S5. Scanning electron microscope images of **A.** SBA-15, **B**. SBA-Eth-SIM, **C**. SBA-AC-SIM, **D**. SBA-AC-SP, **E**. SBA-Eth-SP, **F.** MCM-41, **G**. MCM-AC-SIM, , **H** MCM-Eth-SIM, **I** MCM-AC-SP, J)MCM-Eth-SP, **k** FS, **L** FS-AC-SIM, **M** FS-Eth-SIM, **N** FS-AC-SP, **O** FS-Eth-SP at 20 kX magnification**.** SBA: SBA-15, MCM=MCM-41, FS: fumed silica, Eth: Ethanol, AC: acetone, SIM: solvent impregnation method and SP: electrospraying method

2.5 Particle size distribution

Particle size distributions of the silica materials before and after drug loading are shown in Figure S6, while the corresponding data (including average particle size and span value) are given in Table S3. Particle size deduced from DLS analysis appeared smaller compared to that obtained using SEM, which is most likely due to the sonication process performed prior to DLS measurements. The results demonstrated that electrosprayed mesoporous silica particles (SBA-15 and MCM-41) are nearly uniform in size (span ≤ 0.073) exhibiting smaller particle sizes than raw silica, effect attributed to the impact of atomization of merged fiber-like structures. The mean particle size of pristine SBA-15 and MCM-41 was 1231 and 1611 nm, respectively, whereas for electrosprayed formulations (e.g. SBA-Eth-SP and MCM-Eth-SP), the mean particle size was 535 and 409 nm, respectively. However, the size of electrosprayed non-porous silica formulations (e.g. FS-AC-SP) appeared to be greater than raw particles due to the presence of the dispersed drug crystals, which enhanced particle cohesiveness. Formulations prepared using solvent impregnation (SBA-Eth-SIM, MCM-Eth-SIM and FS-AC-SIM) exhibited increased mean particle sizes of 2091, 2463 and 2496 nm, respectively. In addition, the values D90 of for these particles were 6085, 6811 and 7100 nm, respectively. This increase in particle size and polydispersity (span value $\leq$ 59.9) is attributed to the presence of aggregated particle clusters.

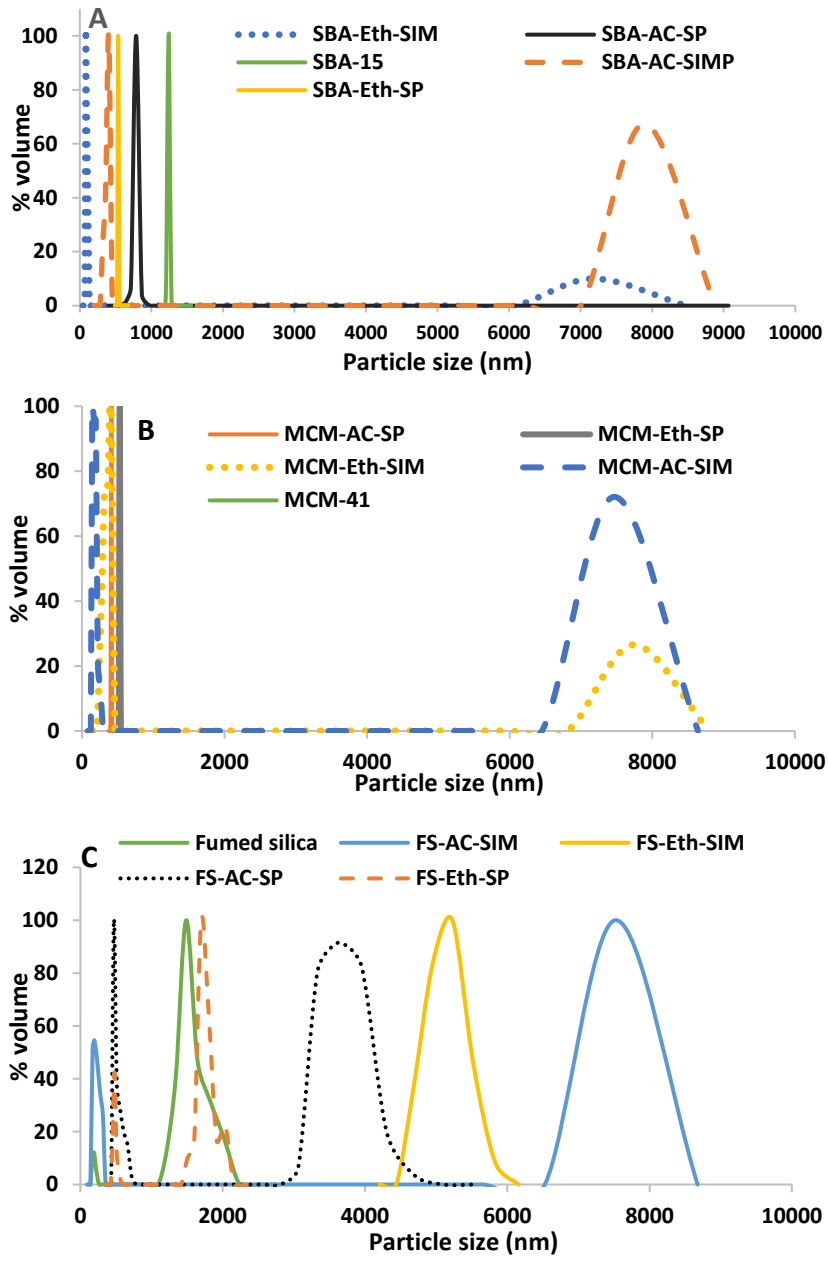

Figure S6. Particle size distribution of **A.** SBA-15, **B.** MCM-41 and **C.** FS based formulations before and after drug loading. SBA: SBA-15, MCM: MCM-41, FS: fumed silica, Eth: Ethanol, AC: acetone, SIM: solvent impregnation method and SP: electrospraying method.

Table S3. Particle size distribution and ζ-potential of different silica particles before and after drug loading

Formulation	D10 (nm)	D50 (nm)	D90 (nm)	Average particle size (nm)	Span value	ζ-potential (mV)
SBA-15	1215	1225	1255	1231	0.03	-42.64 ± 13.72
SBA-AC-SIM	320	400	7600	2773	18.20	-26.05 ± 6.55
SBA-Eth-SIM	90	100	6085.65	2091	59.95	-17.57 ± 5.01
SBA-AC-SP	725	750	780	751	0.07	17.88
SBA-Eth-SP	525	535	547	535	0.04	21.36 ± 3.41
MCM-41	1310	1625	1900	1611	0.36	-54.86 ± 12.97
MCM-AC-SIM	130	170	6900	2400	39.82	-24.0 ± 5.2
MCM-Eth-SIM	250	330	6811	2463.73	19.88	-22.7 ± 17.4
MCM-AC-SP	517	530	536	527.66	0.03	27.26 ± 3.75
MCM-Eth-SP	403	410	414	409	0.02	23.57 ± 12.03
Fumed silica	174	1425	1750	1116.34	1.10	-34.08 ± 13.7
FS-AC-SIM	160	230	7100	2496.67	30.17	-13.45 ± 1.51
FS-Eth-SIM	4610	5000	5370	4993.33	0.15	-12.76 ± 0.09
FS-AC-SP	420	3200	3800	2473.33	1.05	2.68 ± 5.72
FS-Eth-SP	465	1650	1830	1315	0.82	3.94 ± 9.28

2.6 ζ-potential studies

Plain SBA-15, MCM-41 and FS nanoparticles exhibited negative zeta potential owing to the negatively charged silanol groups (SI, Table S4**)**. The ζ-potential values of SBA-15 and MCM-41 nanoparticles were highly negative (-42.64 mV and -54.86 mV, respectively), compared to that of the non-porous FS material (-34.08 mV) [1]. This is attributed to the greater surface area of their mesostructure and thus greater exposure to silanol groups of SBA-15 and MCM-41, when compared to non-porous FS. This suggests that SBA-15 and MCM-41 are highly reactive owing to the large number of surface accessible silanol groups, which are able to electrostatically interact with more drug molecules, hence achieving high drug loading [1]. KAZ3 loading increased the ζ-potential values of all formulations but with variations arising due to the encapsulation method. This might be attributed to the interaction of silica's silanol groups with the positively charged drug molecules. KAZ3 loading on MCM-41 particles using the solvent impregnation technique resulted to an increase in ζ-potential from -54.80 mV to -22.70 mV, whereas the use of electrospraying technique further increased the ζ-potential values of the particles up to 27.26 mV, suggesting a greater interaction between the drug and silanol moieties when compared to the solvent impregnation method. Similar increase in ζ- potential of mesoporous silica particles upon drug loading has been reported previously [2].

Table S4. ζ-potential of the different types of silica particle dispersions in different solvents.

Silica type	Solvent	ζ-potential of dispersion	Stability of dispersion*
SBA-15	Acetone	-9.7 ± 6.5	Unstable
SBA-15	Ethanol	-32.6 ± 6.5	Stable
MCM-41	Acetone	-0.9 ± 6.4	Unstable
MCM-41	Ethanol	-50.7 ± 4.5	Stable
FS	Acetone	-36.7 ± 12.5	Stable
FS	Ethanol	-35.6 ± 9.1	Stable

SBA: SBA-15, MCM: MCM-41, FS: fumed silica, Eth: Ethanol, AC: acetone, SIM: solvent impregnation method and SP: electrospraying method * The separating line between stable and unstable dispersions is normally taken at either +30 or -30 mV. Dispersions with ζ-potential beyond the range of ± 30 was considered stable.

2.7 FTIR studies

FTIR analysis was performed to study the effect of drug loading on the chemical structure or interactions developed between the drug and silica. FTIR spectra (Figure S7) of SBA-15, MCM-41 and FS showed a broad peak at 3420 cm^{-1} that corresponds to O–H stretching vibration of the free silanol groups, while the intense peak in the range of 1000-1100 cm^{-1} is assigned to the stretching vibrations of the Si–O bond [3]. The FTIR spectra of drug-loaded formulations showed all the characteristic drug peaks corresponding to the enone group. This suggests that the chemical structure of KAZ3 is not affected by the electrospraying process. Nevertheless, the decreased intensity and the disappearance of some peaks could be attributed to the dilution effect of silica particles. The FTIR spectra of physical mixtures revealed similar trends, confirming that the reduced peak intensity is indeed due to the dilution effect of the silica particles. The intensities of the peaks corresponding to silanol O–H appear decreased for the

atomized drug loaded formulations as shown in the insert (Figure S7), suggesting that the quantity of free silanol groups has decreased due to their possible interactions with the drug. The reduction or absence of silanol O–H peak intensity due to its consumption during the interaction with the loaded drug or surface functional groups has been previously reported in the literature [4,5].

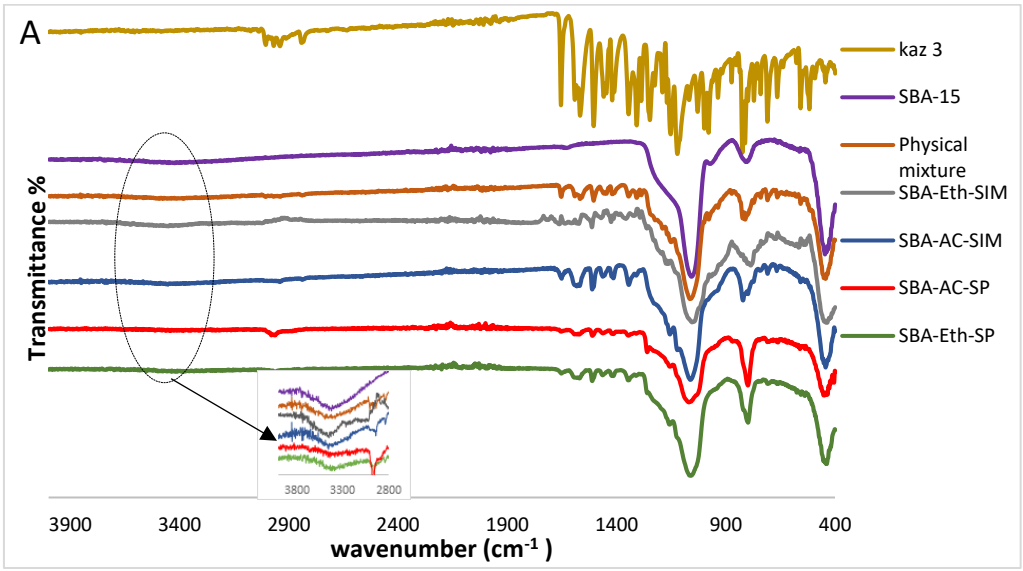
A
kaz 3
SBA-15
Physical mixture
SBA-Eth-SIM
SBA-AC-SIM
SBA-AC-SP
SBA-Eth-SP
Transmittance %
3800 3300 2800
3900 3400 2900 2400 1900 1400 900 400
wavenumber (cm-1)

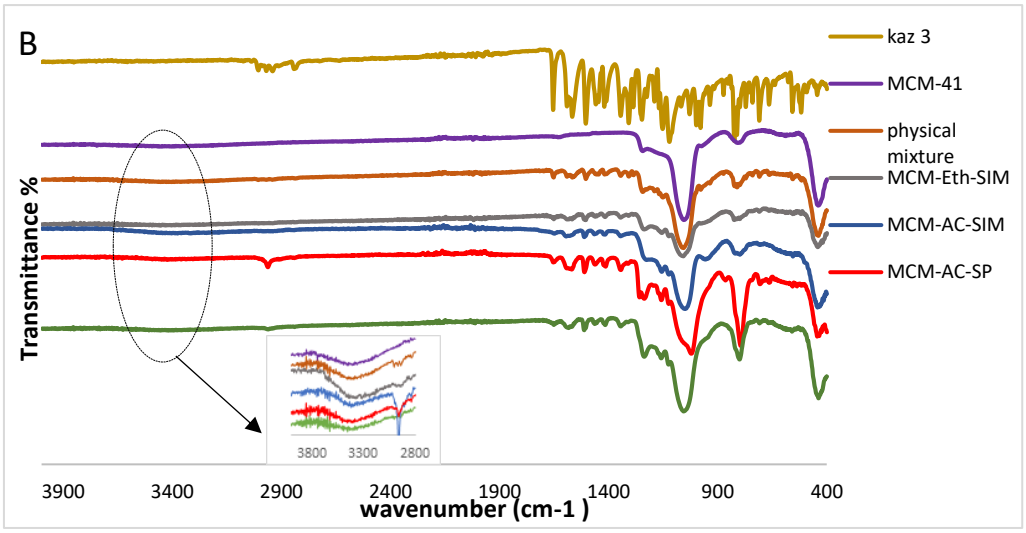
B
kaz 3
MCM-41
physical mixture
MCM-Eth-SIM
MCM-AC-SIM
MCM-AC-SP
Transmittance %
3800 3300 2800
3900 3400 2900 2400 1900 1400 900 400
wavenumber (cm-1)

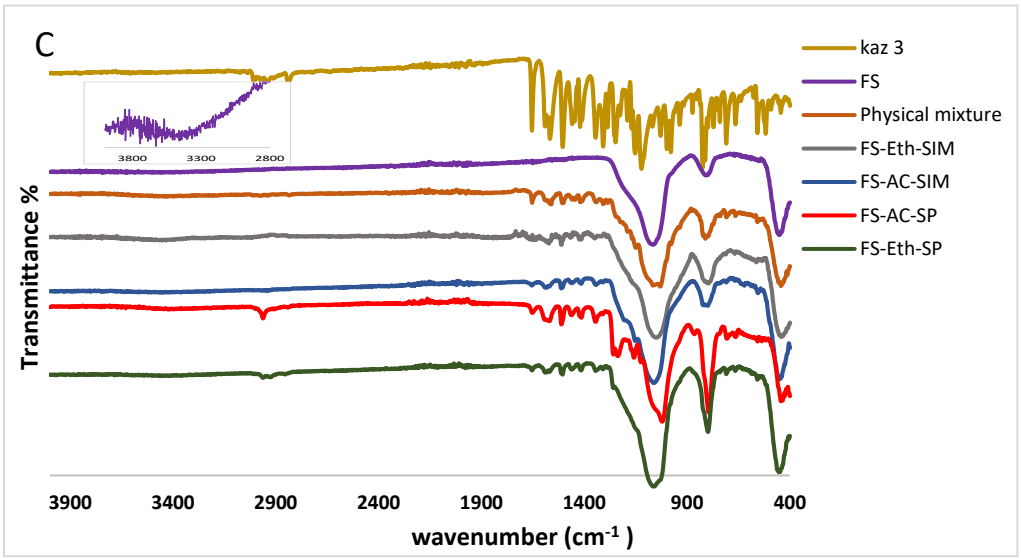
C
kaz 3
FS
Physical mixture
FS-Eth-SIM
FS-AC-SIM
FS-AC-SP
FS-Eth-SP
Transmittance %
3800 3300 2800
3900 3400 2900 2400 1900 1400 900 400
wavenumber (cm-1)

Figure S7. FTIR structure analysis of pure KAZ3 and **A.** SBA-15, **B.** MCM-41 and **C.** fumed silica before and after drug loading, SBA: SBA-15, MCM: MCM-41, FS: fumed silica, Eth: Ethanol, AC: acetone, SIM: solvent impregnation method and SP: electrospraying method

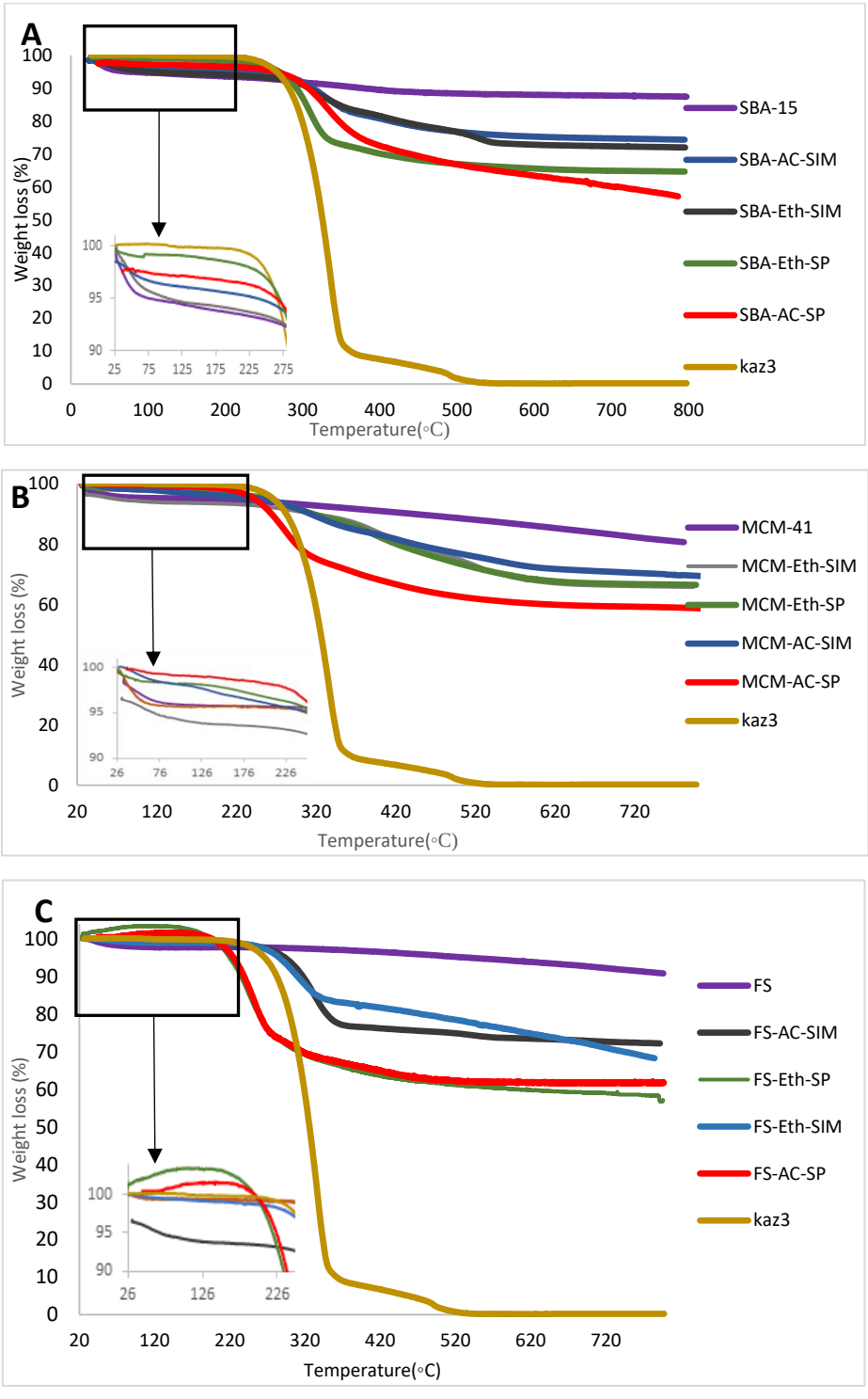

Figure S8. TGA analysis of pure KAZ3 and **A.** SBA-15, **B.** MCM-41 and **C.** fumed silica before and after drug loading. SBA: SBA-15, MCM: MCM-41, FS: fumed silica, Eth: Ethanol, AC: acetone, SIM: solvent impregnation method and SP: electrospraying method

Table S5. Melting points, melting enthalpies and degree of crystallinity obtained from DSC analysis of physical mixtures of KAZ3 with different types of silica particles (SBA-14, MCM-41 or FS) and their corresponding drug loaded formulations.

Type of material	Melting point (°C)	Melting Enthalpy (kJ/mol)	Degree of crystallinity (%)
SBA- KAZ3 physical mixture	98.1	135	100
MCM- KAZ3 physical mixture	98.4	156.3	100
FS-KAZ3 physical mixture	101.18	35	100
SBA-AC-SIM	116 and 93	44.8	33.18
SBA-Eth-SIM	116	107.2	79.40
SBA-AC-SP	92.5	17.5	12.96
SBA-Eth-SP	-	0	0
MCM-AC-SIM	108.2	62.8	40.17
MCM-Eth-SIM	95.8 and 120	132	79.85
MCM-AC-SP	94	24.5	14.82
MCM-Eth-SP	-	0	0
FS-Eth-SIM	94.1	35	100.5
FA-AC-SIM	98.8	17	42.5
FS-AC-SP	94.1	24	60
FS-Eth-SP	95.8	34	85

SBA: SBA-15, MCM: MCM-41, FS: fumed silica, Eth: Ethanol, AC: acetone, SIM: solvent impregnation method and SP: electrospraying method

The shift in drug's melting peak in the physical mixtures from the original drug's melting peak (101 °C) accounts for the entrapment of drug molecules within silica mesopores during the melting process of the DSC procedure. In contrast, the endothermic melting peak shown in thermograms for drug and nonporous silica physical mixture appears at the value identical to drug's melting temperature. The decrease in peak sharpness for the three physical mixtures is due to dilution effect of amorphous silica.

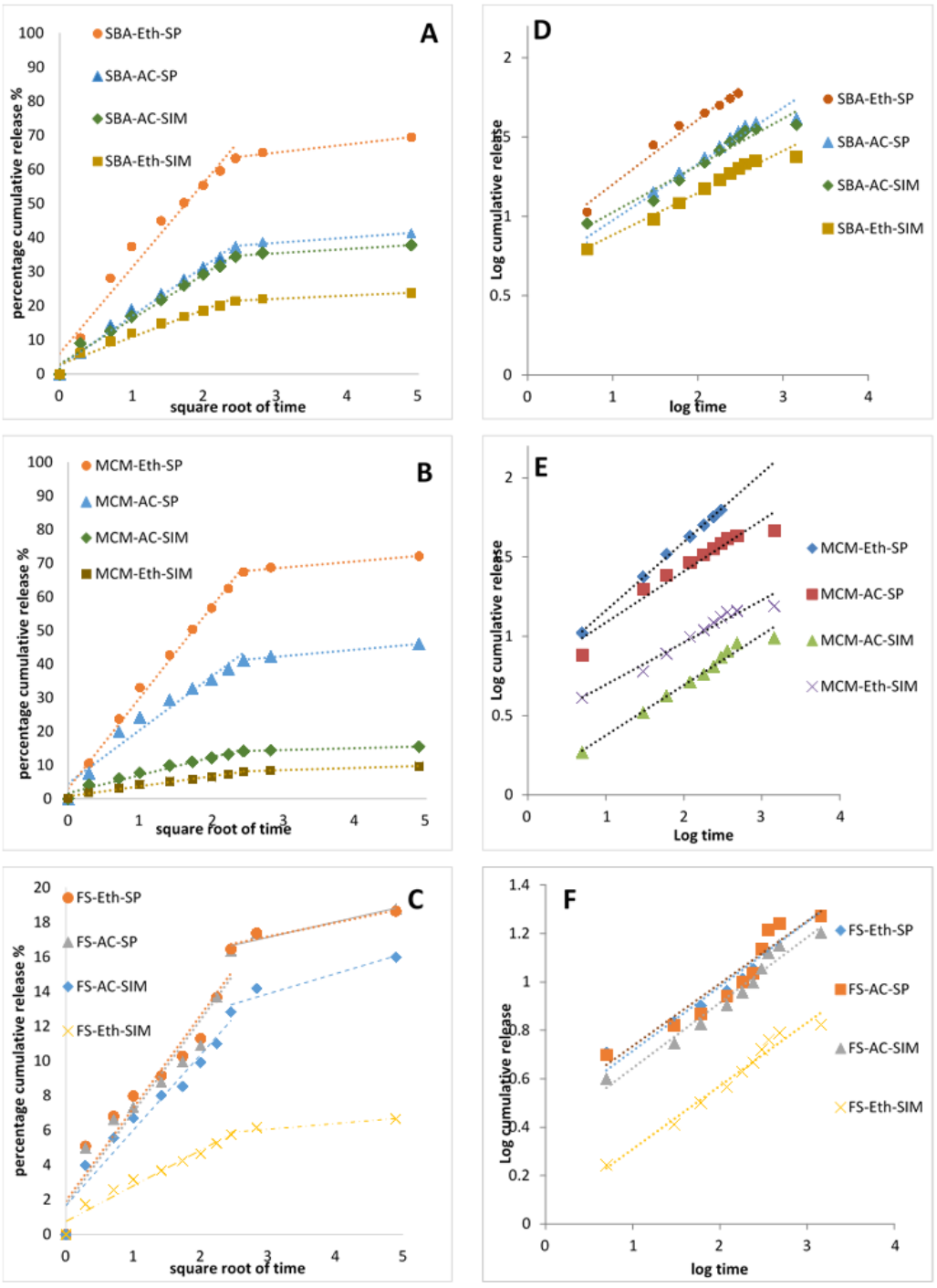

506

507 **Figure S9**. **A., B., C.** Higuchi square root of time plot for the release of KAZ3 from
508 SBA -15, MCM-41 and FS based formulations, respectively. **D., E., F.** Korsmeyer-
509 Peppas model for the *in vitro* KAZ3 release from SBA -15, MCM-41 and FS based
510 formulations, respectively. SBA: SBA-15, MCM: MCM-41, FS: fumed silica, Eth:

Ethanol, AC: acetone, SIM: solvent impregnation method and SP: electrospraying method

Table S6. KAZ3 in vitro release kinetics modelling parameters.

Formulations	Peppas model		Higuchi First step		Higuchi second step	
	R^2	N	R^2	k_H	R^2	k_H
SBA-AC-SIM	0.951	0.29	0.98	13.1	0.96	1.30
SBA-ETH-SIM	0.967	0.26	0.96	7.9	0.98	0.94
SBA-AC-SP	0.955	0.35	0.99	14.5	0.94	1.55
SBA-Eth-SP	0.976	0.41	0.96	24.9	0.98	2.40
MCM-AC-SIM	0.977	0.31	0.97	5.3	0.99	0.54
MCM-Eth-SIM	0.962	0.26	0.98	2.9	0.98	0.64
MCM-AC-SP	0.929	0.32	0.95	15.8	0.99	1.90
MCM-Eth-SP	0.998	0.43	0.99	26.9	0.981	1.83
FS-AC-SIM	0.964	0.27	0.94	4.3	0.91	1.15
FS-Eth-SIM	0.972	0.26	0.96	2.0	0.911	0.32
FS-AC-SP	0.911	0.26	0.91	5.3	0.91	0.88
FS-Eth-SP	0.926	0.25	0.92	5.3	0.93	0.79

SBA: SBA-15, MCM: MCM-41, FS: fumed silica, Eth: Ethanol, AC: acetone, SIM: solvent impregnation method and SP: electrospraying method

24h treatment

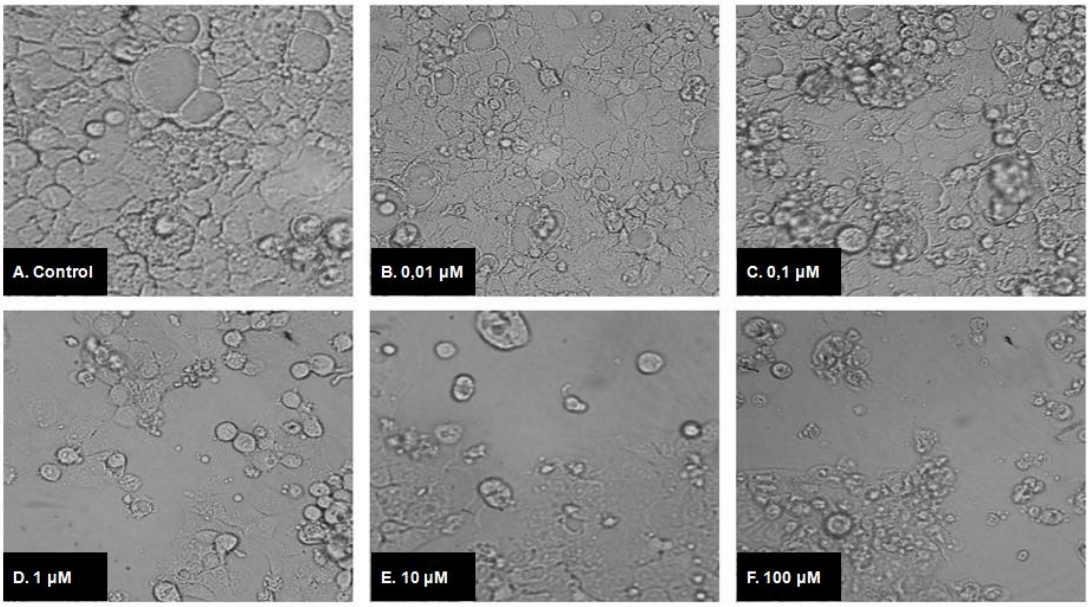

48h treatment

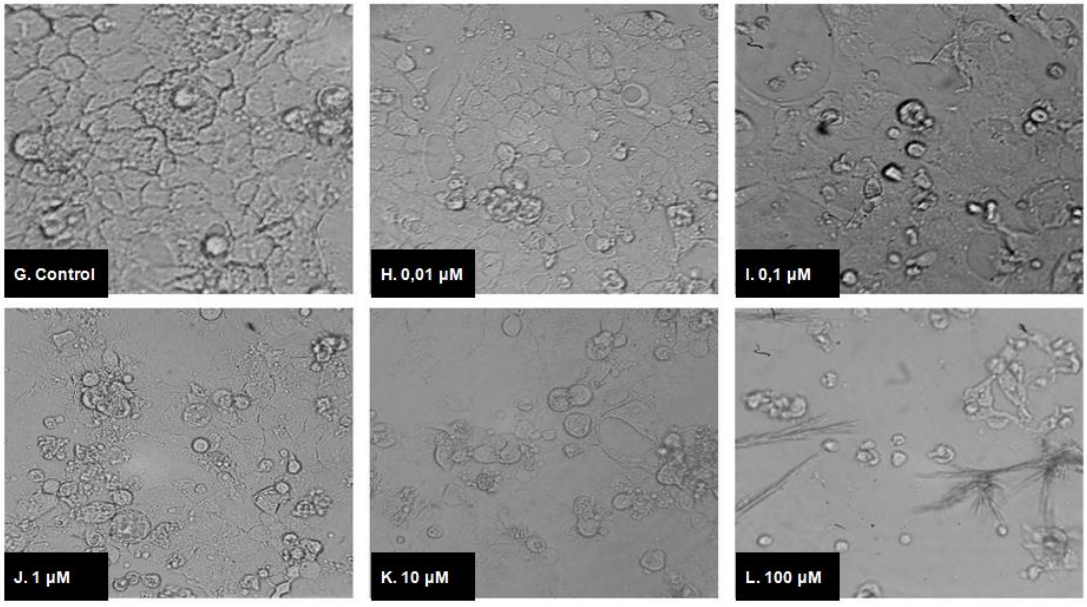

Figure S10. Cellular morphology of Caco-2 cell cultures exposed to KAZ3. Phase contrast microscopic images (32x) of Caco-2 cells grown in the absence (control) or the presence of various concentrations (shown in each panel) of KAZ3 for 24 h and/or 48 h.

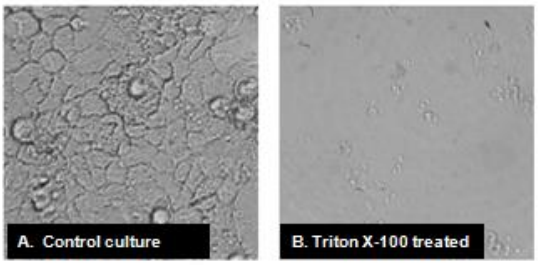

KAZ3-loaded MCM-41 formulations

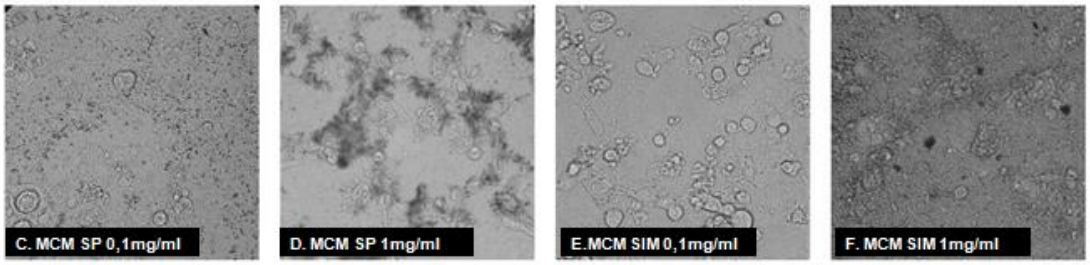

KAZ3-loaded SBA-15 formulations

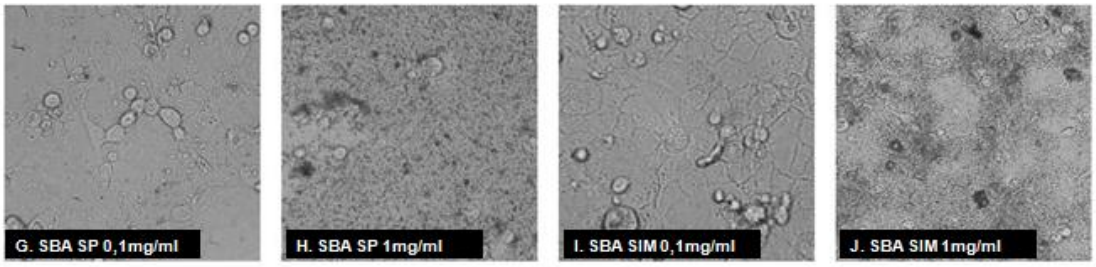

KAZ3-loaded FS formulations

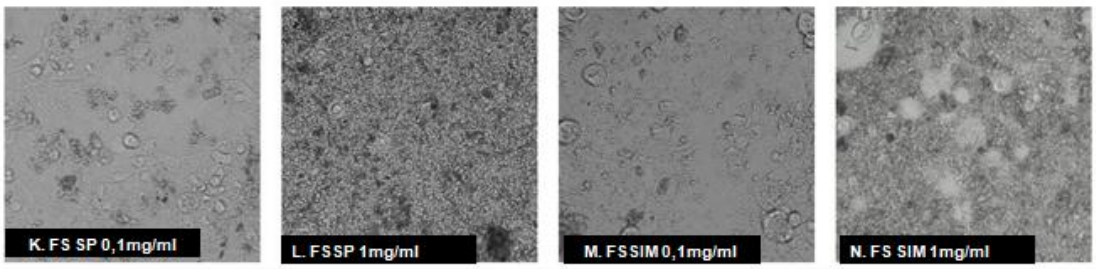

Figure S11. Cellular morphology of Caco-2 cell cultures exposed to KAZ3-loaded MCM, SBA and FS formulations**.** Phase contrast microscopic images (32x) of Caco-2 cell cultures grown **A.** without treatment (control culture) **B**. after treatment with 1 % Triton X-100 and **C**-**N**. after incubation with 0.1 mg/mL and 1 mg/mL of drug loaded MCM, SBA and FS materials for 48 h. [MCM-41, SBA-15: mesoporous silica

nanoparticles; FS: non porous fumed silica nanoparticles; SP: electrospraying method for drug loading; SIM: solvent impregnation method for drug loading.

References

[1] S.A. Jadhav, V. Brunella, G. Berlier, E. Ugazio, D. Scalarone, Effect of Multimodal Pore Channels on Cargo Release from Mesoporous Silica Nanoparticles, J Nanomater. 2016 (2016).

[2] A. Wani, E. Muthuswamy, G.H.L. Savithra, G. Mao, S. Brock, D. Oupický, Surface functionalization of mesoporous silica nanoparticles controls loading and release behavior of mitoxantrone, Pharm. Res. 29 (2012) 2407-2418.

[3] A. Tadjarodi, F. Zabihi, S. Afshar, Experimental investigation of thermo-physical properties of platelet mesoporous SBA-15 silica particles dispersed in ethylene glycol and water mixture, Ceram Int. 39 (2013) 7649-7655.

[4] A. Datt, D. Fields, S.C. Larsen, An experimental and computational study of the loading and release of aspirin from zeolite HY, The Journal of Physical Chemistry C. 116 (2012) 21382-21390.

[5] H.Y. Huang, R.T. Yang, D. Chinn, C.L. Munson, Amine-grafted MCM-48 and silica xerogel as superior sorbents for acidic gas removal from natural gas, Ind Eng Chem Res. 42 (2003) 2427-2433.